

Received May 24, 2019; reviewed; accepted October 13, 2019

Study on bubble characteristics of flotation column in hematite reverse cationic flotation process

Weizhi Wang^{1,2}, Jikang Han¹

¹ College of Mine engineering, North China University of Science and Technology, Tangshan 063009, China

² Mining Development and Safety Technology Key Lab of Hebei Province, Tangshan 063009, China

Corresponding author: jikanghan@163.com (Jikang Han)

Abstract: In the self-designed flotation column simulation system, the foaming characteristics of the micro-bubble countercurrent contact flotation column used in the hematite cation column flotation process are systematically studied. The objective of this study is to investigate the bubble generation by a bubble generator in the flotation column. The bubble image was obtained by the high-speed camera recorder, and the bubble diameter was calculated and analyzed by image processing software. The distribution characteristics of the bubble size under different aeration conditions and with different reagent concentrations were investigated. The results show that as the aeration increases, the average diameter bubbles increases, the bubble size distribution changes from narrow to wide, and the number of small bubbles decreases. The cationic collector GE-609 can change the bubble shape. As the concentration increases, the bubble shape gradually changes from an irregular shape to a standard spherical shape. When the concentration of GE-609 exceeds 2.5 mg/dm³, the average circularity C of the bubbles in the bubble group stabilizes at 1, and the increase in concentration no longer changes the bubble shape. GE-609 also has an efficient foaming effect, as the concentration increases, the bubble diameter distribution changes significantly, the proportion of small bubbles increases, and the proportion of large bubbles decreases significantly. When the critical concentration is exceeded, the bubble diameter distribution probability density peak width no longer changes significantly. Compared with the two types of alcohol foaming agents, GE-609 produces a bubble Sauter diameter close to that of 2-octanol and slightly lower than terpeneol.

Keywords: column flotation, bubble generator, GE-609, circularity, bubble diameter, bubble Sauter diameter

1. Introduction

In order to solve the problems such as complex reagent system, long process and high cost of high-temperature flotation in hematite anionic collector reverse flotation process, the research group has developed hematite cationic (cationic collector-alkyl polypeptide ether, abbreviated as GE-609) reverse flotation process which has simple reagent system and can process at normal temperature flotation. The innovation of this process is that, firstly, a new type of flotation column characterized by high-efficiency recovery of fine mineral particles is introduced. Compared with traditional flotation machine and conventional flotation column, the structure and principle of the flotation column are more effective, which not only has the characteristics of high selectivity and high enrichment ratio of column flotation, but also has the advantages of fine and uniform bubbles in the column, large surface area and more contact opportunities with ore particles under countercurrent conditions due to the introduction of a spray gun micro-bubble generator in the column. Under the premise of ensuring concentrate grade, a higher metal recovery rate can be obtained (Wang et al., 2017). Second, the cationic collector GE-609 used in the process has the advantages of good water solubility, low temperature resistance and good selectivity compared with the conventional cationic collector. More importantly, GE-609 has high

foaming performance that eliminates the need for foaming agents, simplifies floatation agent scheme and saves the costs in industrial applications (Song et al., 2019).

Most of the research on flotation column focuses on application research. In recent years, the research on bubble characteristics in flotation column has been paid more and more attention by scholars at home and abroad. As the main carrier of flotation process, the shape and diameter distribution of bubbles directly affect the selectivity of bubbles and the carrying capacity of carrying target minerals (Eskanolou et al., 2018; Marian and Anna, 2012; Kulkarni and Jyeshtharaj, 2005). The study found that the flotation reagent concentration has a significant effect on the bubble size and shape. The higher the floatation reagent concentration makes, the smaller the bubble diameter is. When the floatation reagent concentration reaches the critical coalescence concentration (CCC), the bubble diameter tends to be stable (Kracht and Rebolledo, 2013; Quinn et al., 2014). Wu. (2002), produces spherical bubbles and ellipsoidal bubbles with the same volume in pure water. It has been found that spherical bubbles move much slower than ellipsoidal bubbles. Dijkhuizen et al. (2005) studied the effect of surfactant on bubble shape and velocity, and proposed that bubble shape control bubble velocity. They believed that surfactants can inhibit the deformation of bubbles and make them more spherical, thus reducing the movement speed of bubbles. Some scholars analyzed the relationship between bubble velocity and gas holdup (ϵ_g) through experiments, and reached the conclusion that low-speed bubbles have a long residence time in the column, which is beneficial to the increase of gas retention (Kracht and Finich, 2010; Rafiei et al., 2011). However, most of the above studies are the effect of the foaming agent on the bubble, and there are few studies on the foaming performance of the collector, which is precisely the key problem of the cationic reverse flotation reagent system. Carrying out research in this area is of great significance both for the optimization of flotation reagents and for the study of the action mechanism of flotation reagents and bubbles.

In this paper, the bubble characteristics of the flotation column in hematite column cationic reverse flotation process are systematically studied in a self-made flotation column simulation system. Based on measuring the average pore diameter of the bubble generator, the distribution characteristics of bubble size generated under different experimental conditions has been studied by using high-speed camera recorder and image processing technology. Meanwhile, the influence of cationic collector on bubble size is primarily explored to obtain the influence of bubble characteristics and reagent concentration on bubble generation in the flotation column. The research results can provide theoretical guidance for structural optimization of bubble generator and industrial application of hematite column flotation process.

2. Materials and methods

2.1. Experimental Design

The experiment is carried out in a flotation column simulation system. The experimental device consists of 6 parts, including simulated flotation column, TS3-100s high-speed video recorder, gas mass flowmeter (MF5706-N-25), lighting system, gas path system and computer data acquisition system as shown in Fig. 1(a). Since the main body of the column is a cylindrical cylinder, the picture is easily distorted when the bubble is taken, so the simulated flotation column is designed as a prism cylinder, the cylinder is 50 mm long, 50 mm wide and 450 mm high, as shown in Fig. 1(b) below. In order to prevent the bubbles from being densely overlapped and to ensure the good shooting effect, an adjustable black baffle is inserted into the analog column to ensure that no overlapping bubbles are captured. A bubble generator (hereinafter referred to as a bubbler) is installed at the bottom of the simulated column. The experiment is carried out at room temperature, during the experiment, water was fed from the upper end of the prism column, and discharged from the bottom end. The liquid volume remained unchanged throughout the process. The gas is fed into the air inlet of the bottom end of the prism column by the air compressor. The aeration amount is adjusted by the gas mass flow meter, and the high-speed camera recorder is used to record the bubble generation in the column bubbler under different operating conditions.

2.2. Data processing

In the experiment, a high-speed camera recorder is used to obtain a bubble image. The focal length of the high-speed camera recorder and the bubbler are kept constant. Alongside that, the aeration valve is

adjusted to a stable aeration amount in the experiment, and the bubble group picture under the aeration condition is recorded after the stable operation of the bubbler. In order to reduce the accidental error, the number of measurements under each aeration condition in the test is more than three times. The extraction of the bubble diameter in the picture is mainly divided into five steps:

- (1) Automatic threshold segmentation algorithm is applied to calculate a threshold in a given image, such as m for the mean and σ for the variance, then the threshold is set to $m+2\sigma$.
- (2) In the segmented image, the black area which is caused by more reflection or hollowness in the bubble is used, and the bubble is subjected to 7 closed operations using the morphological operation to repair and fill the bubble.
- (3) The bubbles fused with the boundary are obtained by the joint region search, and the bubbles and the individual bubbles that are overlapped with each other are distinguished by the area or shape of the bubbles.
- (4) Ellipse detection is performed by using the Hough transform, and the threshold of the Hough transform is set to detect individual bubbles.
- (5) The bubble diameter of the continuous multi-frame bubble image is respectively detected, and statistical analysis is performed according to the size of the different bubble diameters. The bubble equivalent diameter d_i can be expressed as:

$$d_i = \sqrt{\frac{4S_i}{\pi}} \quad (1)$$

$$S_i = \text{The number of pixels occupied by the } i\text{-th bubble} \times \left(\frac{l}{l \text{ the number of pixels}} \right)^2 \quad (2)$$



1-computer; 2-high speed camera recorder; 3-LED lamp; 4-simple flotation column; 5-bubbler; 6-gas mass flow meter; 7-flotation column console; 8-air compressor

Fig 1. (a) Equipment flow chart



Fig. 1. (b) Simulate elevation and side view of flotation column

where S_i is the projected area of the plane after the bubble is imaged, and l is the reference length of the original image.

The average diameter of the bubble under each operating condition is:

$$\bar{d} = \frac{\sum n_i d_i}{\sum d_i} \quad (3)$$

where \bar{d} is average diameter of the bubble, n_i is the number of bubbles with diameter d_i , and d_i is the diameter of the i th bubble (mm).

Referring to the relevant literature (Kracht and Moraga, 2016; Gulden et al., 2018), the Sauter diameter is used to represent the average diameter of the bubble group (d_{32}), which can be defined as:

$$d_{32} = \frac{\sum_{i=1}^n d_i^3}{\sum_{i=1}^n d_i^2} \quad (4)$$

where n is the number of bubbles and d_i is the diameter of the bubble (mm).

3. Results and discussion

3.1. Measurement of the outer diameter of the outer tube of the bubble generator

The foaming of the flotation column is composed of an outer tube and an inner tube. As shown in Figure 2, the frothing mode belongs to microcellular frothing (Ritesh et al., 2018). The outer tube is composed of polymer material with dense micropores on the surface. The average gas-liquid contact angle measured by sampling the surface material of the outer tube is 71.91° , which belongs to a water type bubbler. When the flotation column works, gas is fed into the bottom end of the foaming device by an air compressor, released by air holes on the surface of the inner tube, and then separated out from small holes on the surface of the outer tube of the foaming device to form bubbles. The bubble size in the column is not only affected by the operating conditions, but also by the foam maker's own design. However, there is no relevant data on the pore size distribution of the outer tube of the bubbler. Therefore, it is necessary to extract the outer tube pore size so as to provide the corresponding theoretical basis for the optimization and improvement of the bubbler.

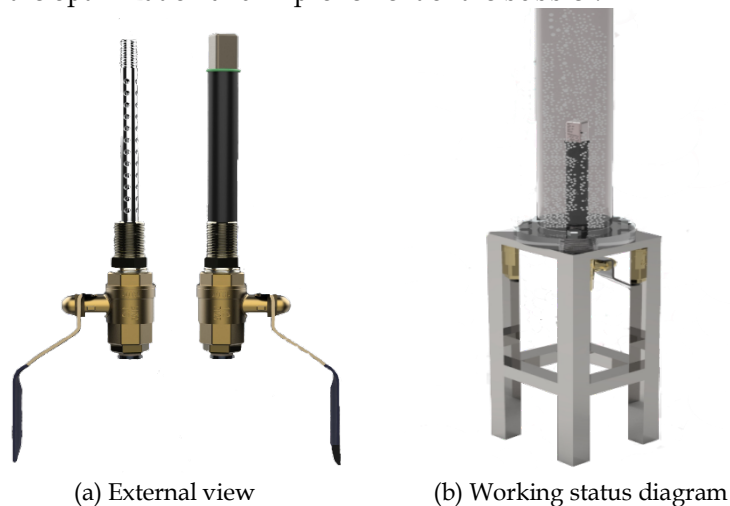


Fig. 2 Bubble generator

As can be seen from Fig. 3, there are obvious differences in the hole pattern and size of each micropore on the outer tube surface of the bubbler. For the size of the aperture, direct measurement cannot be carried out. The method adopted in this paper is to cut the sample at the center of the outer tube of the bubbler, then make the sample into slices, observe the small hole through SEM scanning electron microscope and obtain the picture under the mirror, extract the picture features under the electron microscope using MATLAB, and remove the background, gray scale transformation, median

filtering, threshold segmentation and other operations from the original picture to obtain a clearer image. Fig. 4 shows the pinhole image processed by the original image, counts the diameter of the pore in the image, and obtains the average diameter of the pore through formula (5):

$$d_0 = \frac{\sum_{i=1}^n d_i}{n} \quad (5)$$

where: n is the number of small holes in the SEM image (the number is not less than 100); d_i is the i -th hole diameter (μm) in the SEM image; d_0 is the average diameter of the pore (μm).

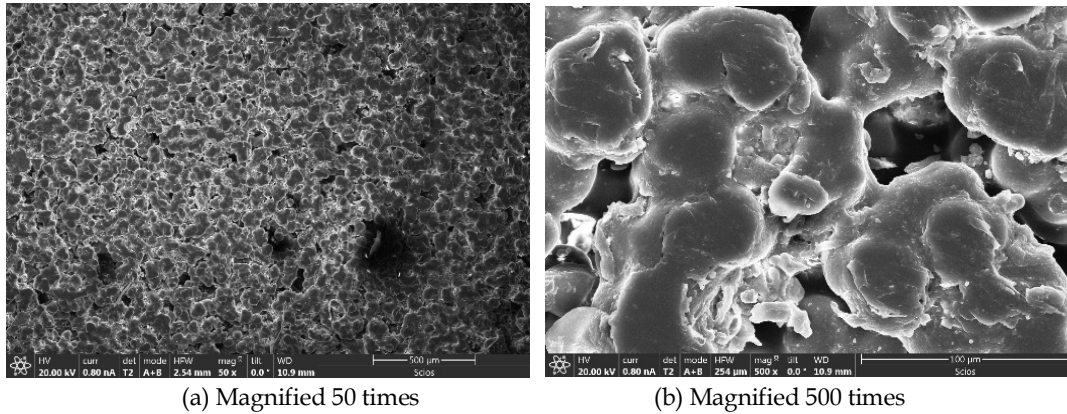


Fig. 3. SEM electron micrograph of outer tube of bubble generator



Fig. 4. Image processing

The processed image can be used to effectively extract the pore size. By using this method, unreasonable pores are removed, and a total of 124 pores with different sizes are obtained, of which the minimum pore size is $51.715 \mu\text{m}$ and the maximum pore size is $502.780 \mu\text{m}$. As can be seen from the distribution rate of small pores given in Fig. 5, the largest number of small pores are in the range of $50\text{--}200 \mu\text{m}$, and only a small number of pores are above $200 \mu\text{m}$. The calculated average pore diameter of small pores is $133.619 \mu\text{m}$.

3.2. Effects of operating conditions on bubbles

3.2.1. Effects of aeration conditions on bubbles

Fig. 6 shows the bubbles generated by the bubbler under different aeration conditions captured by the high-speed video recorder. As it can be seen from the figure, the bubble size gradually increases when the amount of aeration increases. When $Q=0.033 \text{ dm}^3/\text{s}$ and $0.050 \text{ dm}^3/\text{s}$, the bubble size is small and it

is distributed evenly. When $Q=0.067 \text{ dm}^3/\text{s}$, bubbles of large size appear and merge. When $Q=0.083 \text{ dm}^3/\text{s}$, a large number of bubbles collide and merge with each other in violent movement around the bubble generator to form large-size bubbles. The reason is that, under the condition that the liquid volume and the injection pressure difference remain unchanged, the flow rate of the gas through the microporous wall of the specific microporous pipe becomes greater as the gas volume is larger. Anagbo (1990) has proposed that formed bubbles which do not coalesce and decompose can be directly carried away by the current when the gas flow rate is low. In addition, when the gas flow rate is medium, some small bubbles can form into large bubbles. When the gas flow rate is high, the bubbles can directly coalesce into large bubbles.

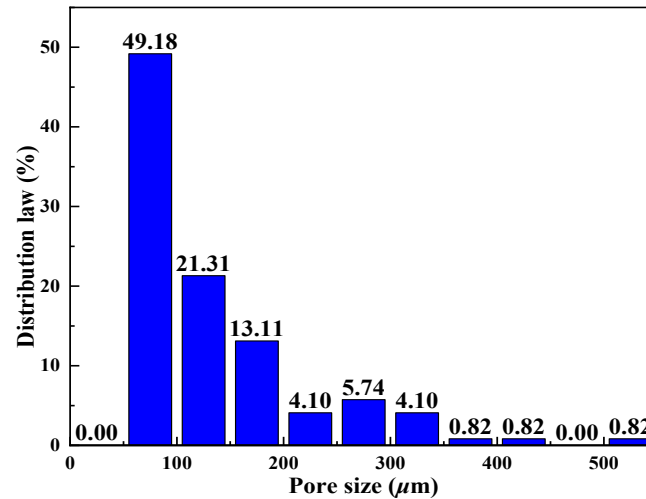


Fig. 5. Outer tube pore distribution law

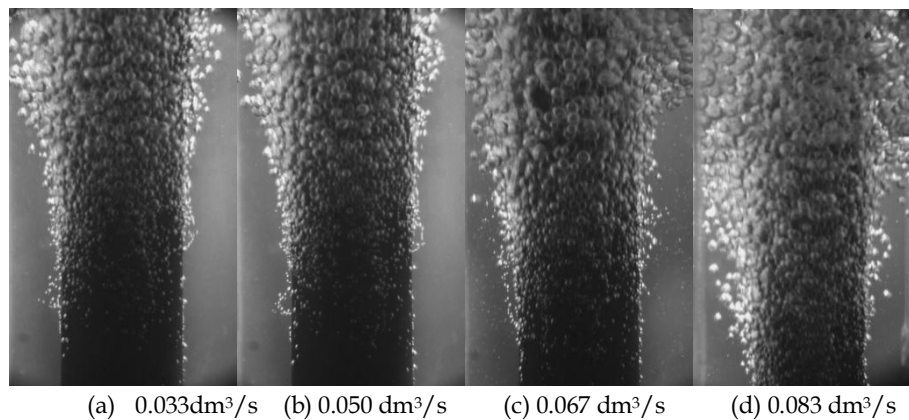


Fig. 6. Influence of air volume on bubble size

Fig. 7 shows the diameter distribution rate and cumulative distribution rate of bubble generation in the bubbler under different aeration conditions. The square column indicates the distribution ratio of different diameters, and the curve indicates the cumulative distribution rate. It can be seen that the bubble generated by the bubbler is a group of bubble clusters, and the bubble size satisfies a certain distribution rule: under a small aeration amount, the micro-bubbles (defining the bubble diameter $< 1 \text{ mm}$ is a micro-bubble (Brittle et al., 2015; Parmar and Majumder, 2013)) have a high proportion. The proportion of large bubbles is very low; as the amount of aeration increases, the proportion of micro-bubbles decreases, the proportion of large bubbles increases gradually, and the normal distribution of bubble sizes becomes more and more obvious.

3.2.2. Effect of flotation reagent on bubble shape

In order to investigate the effect of flotation reagents on bubble characteristics, bubble characteristics under the conditions of clear water and adding cationic collector GE-609 were studied respectively. Figure 8 shows continuous frame bubble images taken under different conditions under clear water.

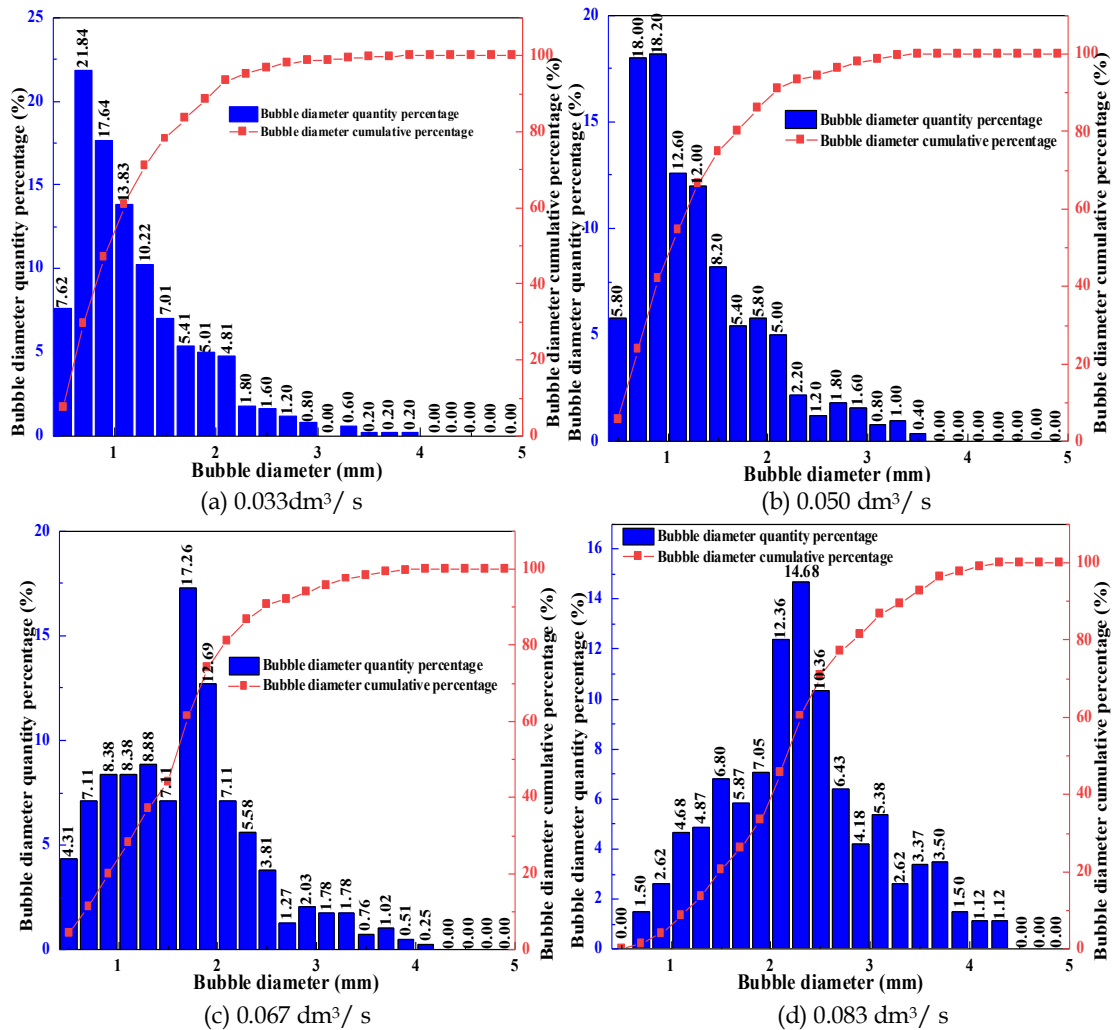


Fig. 7. Bubble diameter distribution under different air charging conditions

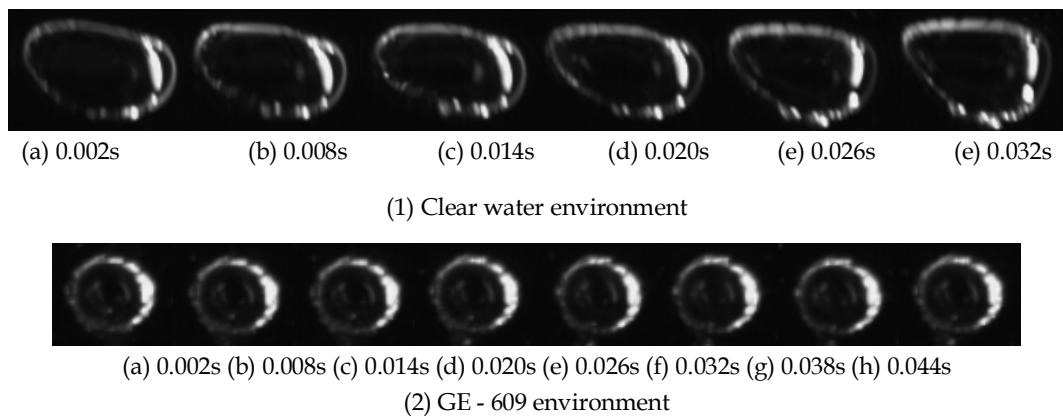


Fig. 8. Bubble shape change in flotation column

It can be seen from Fig. 8(1) that the bubbles in clean water show irregular shapes. with the change of time, the bubbles deform irregularly. However, GE-609 with a certain concentration is added to Fig. 8(2), which shows that the shape and size of the bubbles no longer change obviously with the change of time, showing a more regular circle. By introducing circularity C , the shape of the bubbles under different floatation reagent concentrations can be quantitatively described (Wibawa et al., 2019). The image analysis and circularity calculation program compiled by MATLAB language is used to extract and calculate bubble shapes in bubble groups under different conditions. The calculation formula is as follows:

$$C = \frac{2\sqrt{\pi S}}{P} \quad (6)$$

where: S is the bubble area, P is the bubble perimeter, C is the bubble roundness value, and the closer the C is to 1, the closer the bubble is to the circle.

After a series of processing of the original image, the circularity value of the bubble is obtained. As shown in Fig. 9, based on massive running calculations, it is found that when the circularity of the bubble is less than 0.5, it is usually overlapping bubble and adhesive bubble. Therefore, the circularity threshold value is appropriately adjusted to exclude overlapping bubbles. Finally, the data are collected and collated to obtain the average circularity value of the bubble under different floatation reagent concentrations.

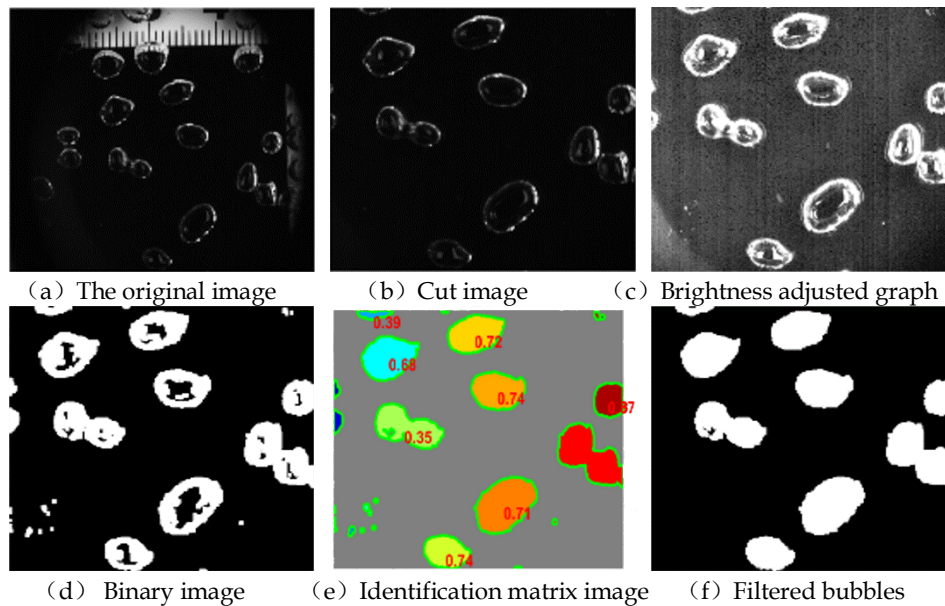


Fig. 9. Flowchart of image processing

Through statistics and sorting, the average circularity of bubbles under different concentrations is obtained, and the variation rule of the average circularity of bubbles with the concentration of flotation reagent GE-609 is shown in the figure. In Fig. 10, it can be observed that the change of circularity can be divided into two sections. The first section increases the circularity of the bubble as the concentration increases, and the bubble is more and more close to a regular sphere. In the second stage, with the further increase of concentration, the circularity value of the bubble does not change any more, the circularity value C is stable at about 1, and the bubble is regular spherical. At this point, the concentration only changes the size of the bubble and does not change the shape of the bubble.

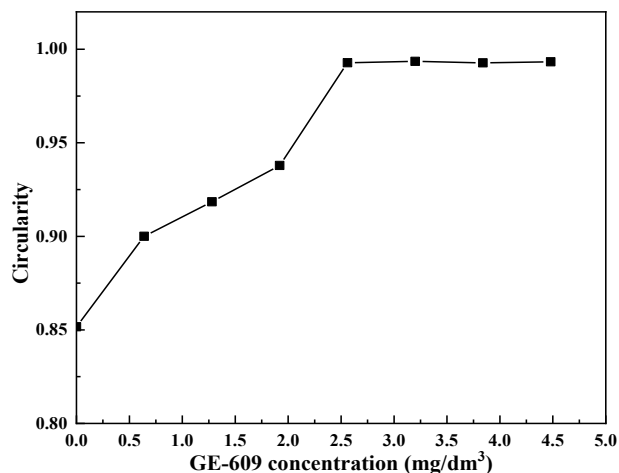


Fig. 10. Average circularity value of bubble group under different GE-609 concentration

3.2.3. Effect of flotation reagent on size distribution

Fig. 9(a) shows the bubbles extracted from the capture zone of the flotation column when the aeration volume is $0.067 \text{ dm}^3/\text{s}$. Since the water in the clean water environment has a large surface tension, the generated small bubbles merge and break continuously during the rising process, so the bubbles rise to the capture zone to form a small number of large bubbles with low mechanical strength. In the flotation column, the area from the ore feeding port to the bottom of the column is a mineralized area. Obviously, a small amount of large bubbles in the column cannot meet the needs of industrial operations.

Fig. 11 shows the effect of GE-609 concentration on bubble diameter. It can be seen from the figure that GE-609 concentration has a significant effect on bubble diameter. In clean water environment, the bubble diameter distribution is wide, ranging from 1mm to 7 mm. The size of the bubble added with GE-609 changes significantly. At low concentration, the content of large and small bubbles is higher, the difference between the content of medium-sized bubbles and that of "two sides" bubbles is not large, and the bubbles are distributed in a dispersed state. When the concentration is $0.64 \text{ mg}/\text{dm}^3$, the average bubble diameter is 2.5 mm. When the concentration increases to $1.28 \text{ mg}/\text{dm}^3$, the bubble diameter decreases to about 2 mm, the content of small bubbles increases significantly, and the distribution range of bubble diameter narrows. With the continuous increase of the concentration, the "density peak" of bubble diameter distribution gradually shifts to the left, and the distribution range of bubble diameter further decreases. When it reaches $3.2 \text{ mg}/\text{dm}^3$, the bubble diameter decreases to about 1mm and the diameter is relatively uniform.

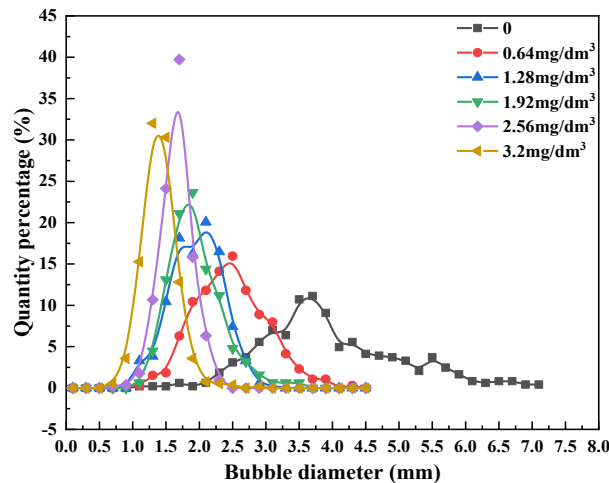


Fig. 11. Effect of GE-609 concentration on bubble diameter

In order to further explore the effect of collector GE-609 on the bubble diameter, the concentration of GE-609 continuously increased, and GE-609 was compared with 2-octanol and terpineol, two efficient foaming agents. The study found that with the increase of collector concentration, the density peak of bubble diameter distribution further contracted and moved to the left. When the concentration reached a fixed value, the density peak width no longer changed. When GE-609 concentration exceeds $10.24 \text{ mg}/\text{dm}^3$, it can be seen from the Fig. 12 that the peak width of bubble diameter distribution density no longer changes significantly.

The effect of three agents on bubbles is further compared. Sauter diameter is taken as the average diameter of the bubble group. It is found from the Sauter variation rule chart with flotation agent concentration in Fig. 13 that with the increase of agent concentration, the bubble Sauter diameter curve drops sharply. When the agent concentration increases to a fixed value, the curve presents an inflection point. At this point, the effect of the increase of agent concentration on the bubble Sauter diameter decreases significantly, and Sauter diameter no longer changes significantly. This inflection point is the CCC value of the agent. The CCC values of 2-octanol and terpineol foaming agents are $8.0 \text{ mg}/\text{dm}^3$ and $12.8 \text{ mg}/\text{dm}^3$ respectively, and GE-609 is between them $11.2 \text{ mg}/\text{dm}^3$. When the three agents reach the critical concentration value, the Sauter diameters corresponding to 2-octanol, terpineol and GE-609 are 0.5 mm, 0.5 mm and 0.54mm respectively, indicating that GE-609 is similar to 2-octanol and slightly stronger than terpineol in inhibiting bubble Sauter diameter.

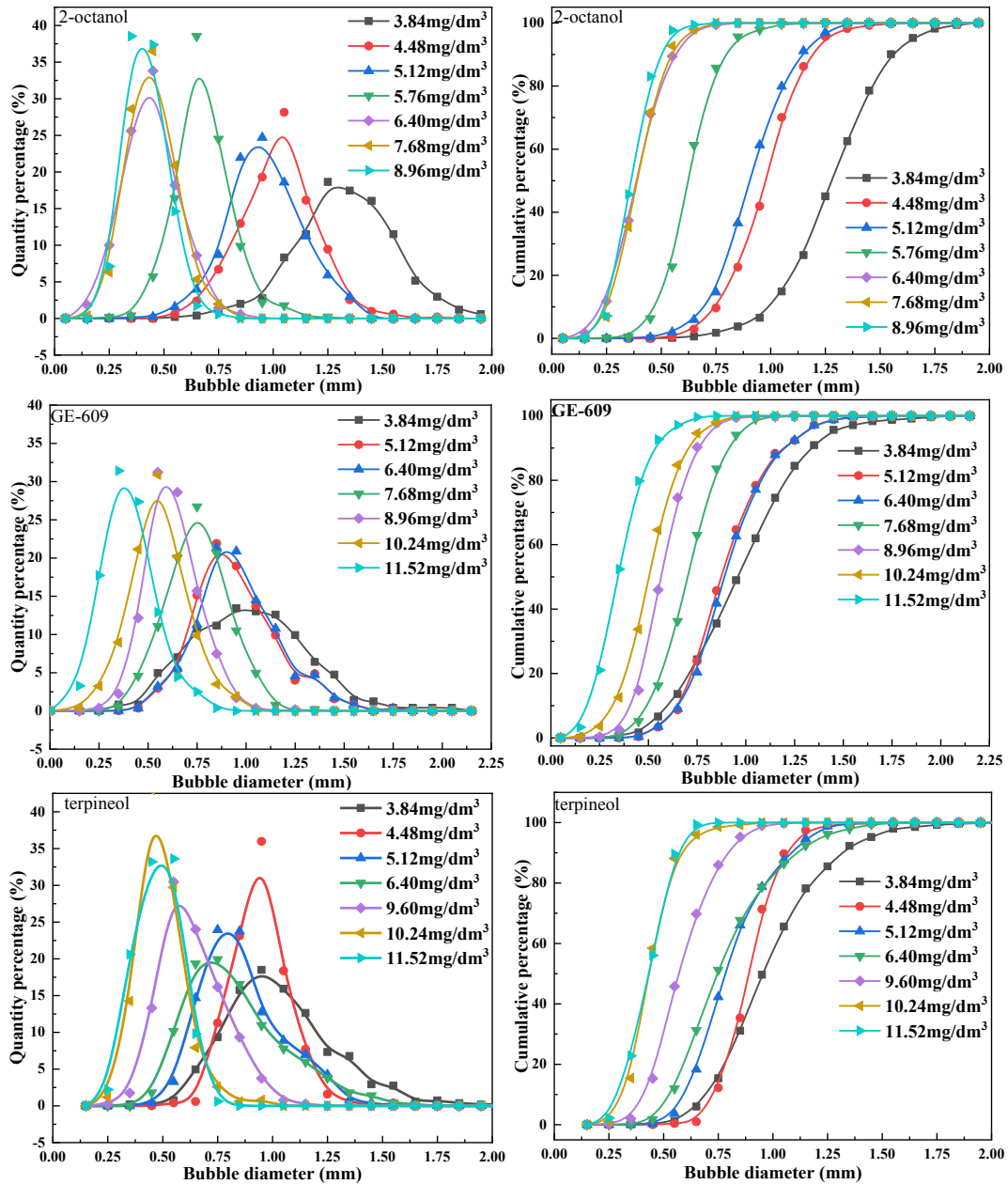


Fig. 12. Effect of flotation reagents on bubble diameter distribution

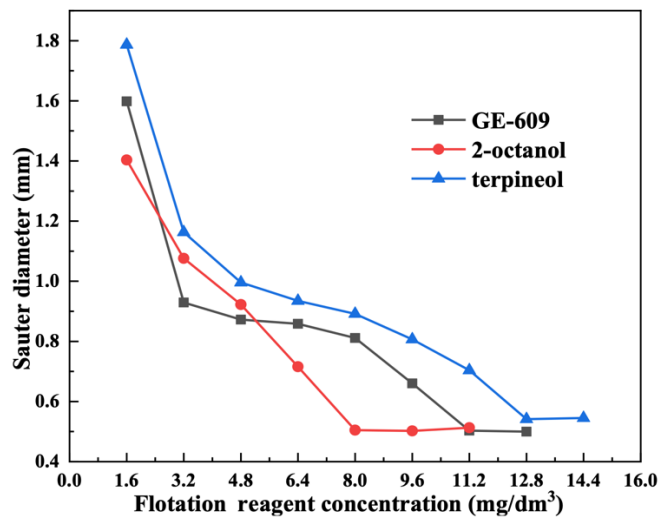


Fig. 13. Effect of flotation reagent concentration on bubble Sauter average diameter

4. Conclusions

- (1) In the micro-bubble countercurrent contacting flotation column, the hydrophilic material surface of the spray gun type bubble generator has micro holes with different sizes, the aperture range is 50-500 μm , and the average aperture is 133.619 μm ; Adjusting the appropriate aeration amount can produce relatively uniform tiny bubbles.
- (2) The amount of aeration has a significant effect on the size of bubbles in the flotation column. Keeping the liquid volume constant in the column, the larger the aeration volume is, the wider the bubble size distribution and the smaller the number of micro-bubbles is; the diameter distribution of the generated bubbles satisfies the normal distribution characteristics.
- (3) Collector GE-609 can change the bubble shape. With the increasing concentration, the bubble gradually changes from irregular shape to stable spherical shape. When the concentration reaches a fixed value, the bubble shape will not change any more.
- (4) Collector GE-609 has high foaming performance. With the increase of concentration, the bubble diameter range changes from wide to narrow. When reaching a fixed value, the bubble diameter distribution is basically unchanged. Compared with 2-octanol and terpineol foaming agents, the CCC values of 2-octanol, GE-609 and terpineol are 8 mg/dm^3 , 11.2 mg/dm^3 and 12.8 mg/dm^3 respectively, and the Sauter diameter of bubbles generated by GE-609 and 2-octanol is slightly smaller than that of terpineol in inhibiting bubble diameter.

Acknowledgments

The authors would like to express their gratitude for the financial support from the Provincial Natural Science Fund of China Hebei (E2017209214) and the authors are grateful to the Mining Development and Safety Technology Key Lab of Hebei Province for its technical support.

References

- ANAGBO, P.E., BRIMACOMBE, J. K., 1990. *Plume characteristics and liquid circulation in gas injection through a porous plug*. Metallurgical Transactions B. 21, 04, 637-648.
- BRITTLE, S., DESAI, P., N.G., W.C., DUNBAR, A., HOWELL, R., TESARR, V., ZIMMERMAN, W.B., 2015. *Minimising micro-bubble size through oscillation frequency control*. Chemical Engineering Research & Design. 104, 357-366.
- DIJKHUIZEN, W., HENGEL, E., DEEN, N.G., 2005. *Numerical investigation of closures for interface forces acting on single air bubbles in water using volume of fluid and front tracking models*. Chemical Engineering Science. 60, 22, 6169-6175.
- ESKANLOU, A., KHALES, M.R., ABDOLLAHY, M., 2018. *Bubble loading profiles in a flotation column*. Physicochemical Problems of Mineral Processing. 54, 2, 355-362.
- GULDEN, S. J., RIEDELE, C., ROLLIE, S., KOPF, M.-H., NIRSCHL, H., 2018. *Online bubble size analysis in micro flotation*. Chemical Engineering Science. 185, 168-181.
- KRACHT, W., FINICH, J. A., 2010. *Effect of frother on initial bubble shape and velocity*. International Journal of Mineral Processing. 94, 03-04, 115-120.
- KRACHT, W., MORAGA, C., 2016. *Acoustic measurement of the bubble Sauter mean diameter d_{32}* . Minerals Engineering. 98, 122-126.
- KRACHT, W., REBOLLEDO, H., 2013. *Study of the local critical coalescence concentration (l-CCC) of alcohols and salts at bubble formation in two-phase systems*. Minerals Engineering. 50, 77-82.
- KULKARNI, A.A., JYESHTHARAJ, J.B., 2005. *Bubble formation and bubble rise velocity in gas-liquid systems: a review*. Industrial and Engineering Chemistry Research. 44, 16, 5873-5931.
- MARIAN, B., ANNA, M., 2012. *The distribution of air bubble size in the pneumo-mechanical flotation machine*. Archives of Mining Sciences. 57, 03, 729-740.
- PARMAR, R., MAJUMDER, S.K., 2013. *Micro-bubble generation and micro-bubble-aided transport process intensification-a state-of-the-art report*. Chemical Engineering. 64, 79-97.
- QUINN, J.J., SOVECHLES, J.M., FINICH, J.A., 2014. *Critical coalescence concentration of inorganic salt solutions*. Minerals Engineering. 58, 1-6.
- RAFIEI, A.A., ROBERTZE, M., FINICH, J. A., 2011. *Gas holdup and single bubble velocity profile*. International Journal of Mineral Processing. 98, 89-93.

- RITESH, P., SUBRATA, K.M., ANUGRAH, S., 2018. *Flotation technique: Its mechanisms and design parameters*. Chemical Engineering and Processing-Process Intensification. 127, 249-270.
- SONG, Z.X., HAN, J.K., WANG, W.Z., ZHANG, R.H., LI, X., 2019. *Development and application status of flotation column technology*. Metal Mine. 6, 20-26.
- WANG, W.Z., LIU, Z.W., LAI, Y.B., 2017. *Experimental Study on cationic reverse flotation by flotation column of a magnetite and hematite mixed iron ore*. Multipurpose Utilization of Mineral Resources. 6, 64-67.
- WIBAWA, E. J., ARIF, W., OKTO, D., 2019. *Hydrodynamic characteristics of the micro-bubble dissolution in liquid using orifice type micro-bubble generator*. Chemical Engineering Research and Design. 141, 01, 436-448.
- WU, M.M., 2002. *Experimental studies on the shape and path of small air bubbles rising in clean water*. Physics of Fluids. 14, 07, 49-52.